Accepted Manuscript

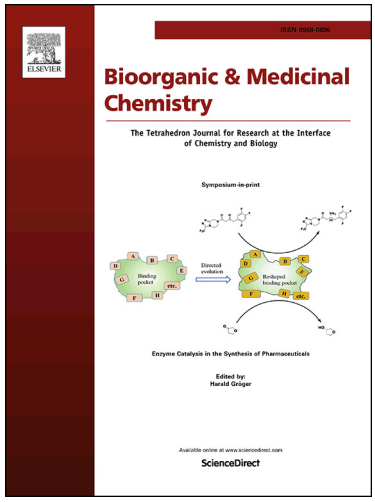

Discovery and development of novel rhodanine derivatives targeting enoyl-acyl carrier protein reductase

Jian-Fei Xua, Tian-Tian Wang, Qing Yuan, Yong-Tao Duan, Yun-Jie Xu, Peng-Cheng Lv, Xiao-Ming Wang, Yu-Shun Yang, Hai-Liang Zhu

PII: S0968-0896(19)30059-8
DOI: https://doi.org/10.1016/j.bmc.2019.02.043
Reference: BMC 14779

To appear in: *Bioorganic & Medicinal Chemistry*

Received Date: 11 January 2019
Revised Date: 18 February 2019
Accepted Date: 20 February 2019

Please cite this article as: Xua, J-F., Wang, T-T., Yuan, Q., Duan, Y-T., Xu, Y-J., Lv, P-C., Wang, X-M., Yang, Y-S., Zhu, H-L., Discovery and development of novel rhodanine derivatives targeting enoyl-acyl carrier protein reductase, *Bioorganic & Medicinal Chemistry* (2019), doi: https://doi.org/10.1016/j.bmc.2019.02.043

Discovery and development of novel rhodanine derivatives targeting enoyl-acyl carrier protein reductase

Jian-Fei Xua[a,†], Tian-Tian Wang[a,†], Qing Yuan[a], Yong-Tao Duan[b], Yun-Jie Xu[a], Peng-Cheng Lv[a], Xiao-Ming Wang[a,*], Yu-Shun Yang[a,*], Hai-Liang Zhu[a,*]

[a]State Key Laboratory of Pharmaceutical Biotechnology, Nanjing University, Nanjing 210023, China

[b]Henan Provincial Key Laboratory of Children's Genetics and Metabolic Diseases, Children's Hospital Affiliated to Zhengzhou University, Zhengzhou Children's Hospital, Zhengzhou, 450018, China

[†]Both authors contributed equally to the work

[*]Corresponding author. Tel. & Fax: +86-25-89682572; E-mail: zhuhl@nju.edu.cn; ys_yang@nju.edu.cn; wangxm07@nju.edu.cn.

Abstract:

A series of rhodanine derivatives **RB1-RB23** were synthesized through a two-round screening. Their *Mycobacterial tuberculosis* (*Mtb*) InhA inhibitory activity and *Mtb* growth blocking capability were evaluated. The most potent hit compound **RB23** indicated comparable InhA inhibiton (IC_{50} = 2.55 μM) with the positive control Triclosan (IC_{50} = 6.14 μM) and Isoniazid (IC_{50} = 8.29 μM). Its improved growth-blocking effect on *Mtb* and low toxicity were attractive for further development. The docking simulation revealed the possible binding pattern of this series and picked the key interacted residues as Ser20, Phe149, Lys165 and Thr196. The 3D-QSAR model visualized the SAR discussion and hinted new information. Modifying the surroundings near rhodanine moiety might be promising attempts in later investigations.

Keywords:

Bacterial Infection; InhA Inhibition; Computer Assistant Drug Design; Rhodanine; Molecular Docking; 3D-QSAR

1. Introduction

Bacterial infection is a nonnegligible risk worldwide and it has become even more dreadful because of drug resistance and clinical complication.[1-3] With increasing knowledge of antibacterial targets and corresponding interactions, the development of potent drug candidates gradually infers some traces to follow.[4-6] One available strategy is blocking the fatty acids biosynthesis of the pathogens.[7-9] All through this pathway, enoyl-acyl carrier protein reductase (InhA) is a convinced target for treating tuberculosis by the first-line drug isoniazid.[10-12] Being highly conserved and distinguished from the mammalian fatty acid biosynthesis enzymes, InhA is suitable as such a target.[13-15] When computer assistant drug design (CADD) seems more popular recently in medicinal chemistry, a variety of InhA inhibitory series have been produced, such as triclosan[16,17], isoniazid-NAD analogues[18], pyrrolidine carboxamides [19,20], triazoles[21,22] and pyridomycin[23,24]. Glancing at them, a typical purpose to inhibit InhA was curing tuberculosis[19,22,24]. Since drug discovery for tuberculosis upon common routes such as protein synthesis, cell wall, DNA gyrase and ATP synthesis faces problems including resistance and poor selectivity[25,26], blocking fatty acids biosynthesis at InhA seemed a promising choice[27,28]. Though designed for InhA, the *in vitro* inhibition of present inhibitors on *Mycobacterial tuberculosis* (*Mtb*) still need to be improved.[29] Therefore, exploiting new hit compounds for InhA to treat tuberculosis is in urgent emergency.[30,31]

In this work, we started our series from the rhodanine moiety because of its reported biological activities. Its bacterial-relating targets include penicillin-binding proteins[32], RNA polymerase[33,34], oxyreductase enzymes[35], and especially, the fatty acid biosynthesis related ones such as *Plasmodium falciparum* FabI [36] and then InhA [37]. By employing the similarities of previous work, we modified the detail of the linker to introduce stretched group as shown in Figure 1. Seeking the new possibilities of group B from amino acid residues and alkyl chains, we set it as a aryl one to further balance the requirements of both group A and B. This strategy with a two-round screening might raise new information during the comparisons between both the bioactivities and molecular docking results. Through the improving procedure round by round, this work might infer hints for future development of InhA inhibitors.

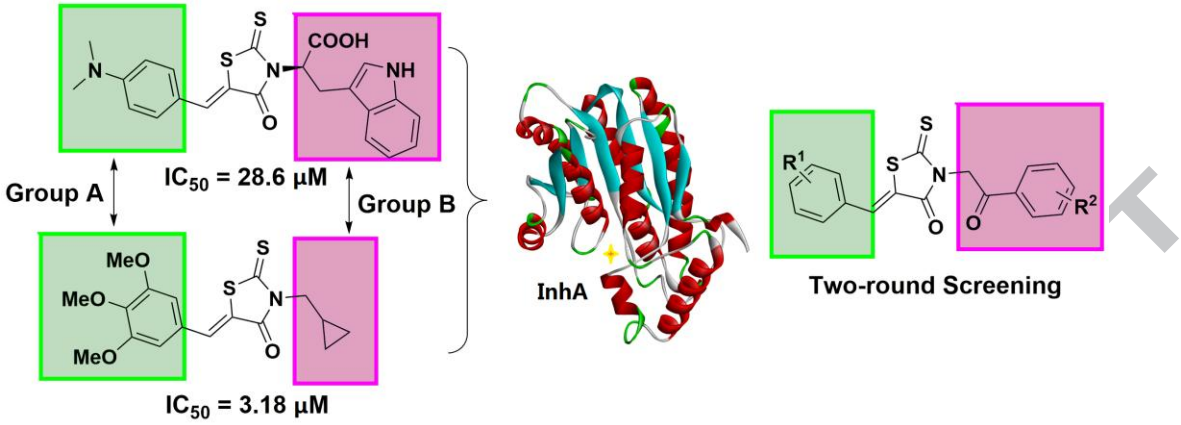

Figure 1. The designing concept of the novel series as InhA inhibitors.

2. Results and discussion

2. 1. Chemistry

The general synthesis route and the structures of the rhodanine derivatives **RB1-RB23** were shown in Scheme 1. All of them except (**RB7**[38] and **RB9**[39]) were synthesized for the first time. A series of substituted benzaldehyde, rhodanine and urea were mixed and stirred in ethanol to acquire intermediate **B**. Then the following reaction with different bromoacetophenones and sodium ethylate resulted in the corresponding target compounds. Compounds **RB16-RB23** were derived according to the preliminary Structure-Activity Relationship (SAR) of **RB1-RB15**. Recrystallisation was performed to guarantee the refined compounds gave satisfactory analytical and spectroscopic data. Since the spectroscopic data of the synthesized compounds did not show obvious isomerism, we carefully checked them and made comparison with reported ones (including **RB7**[38] and **RB9**[39]) to confirm that the compounds in this work were all *trans*-forms.

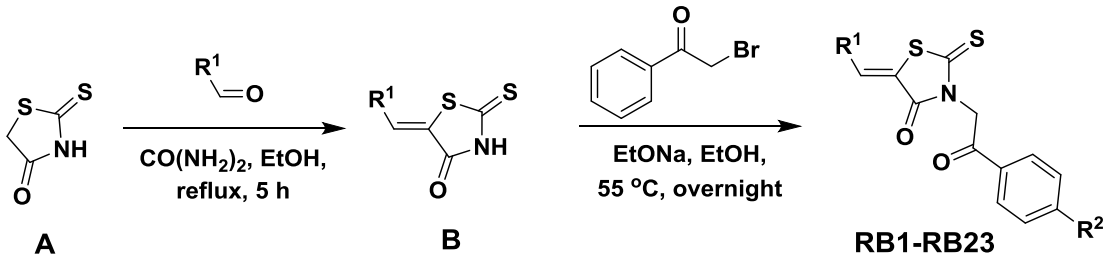

Code	R^1	R^2	Code	R^1	R^2
RB1	Phenyl	H	**RB13**	2-Methoxyphenyl	H

RB2	4-Fluorophenyl	H	**RB14**	3-Methoxyphenyl	H
RB3	4-Chlorophenyl	H	**RB15**	3,4,5-Trimethoxyphenyl	H
RB4	4-Bromophenyl	H	**RB16**	4-Fluorophenyl	OMe
RB5	*p*-Tolyl	H	**RB17**	4-Chlorophenyl	OMe
RB6	4-Methoxyphenyl	H	**RB18**	4-Bromophenyl	OMe
RB7	4-Nitrophenyl	H	**RB19**	*p*-Tolyl	OMe
RB8	4-Hydroxyl	H	**RB20**	2-Chlorophenyl	OMe
RB9	4-Dimethylaminophenyl	H	**RB21**	3-Chlorophenyl	OMe
RB10	4-Acetamidephenyl	H	**RB22**	2-Methoxyphenyl	OMe
RB11	2-Chlorophenyl	H	**RB23**	3,4,5-Trimethoxyphenyl	OMe
RB12	3-Chlorophenyl	H			

Scheme 1. General synthesis of **RB1-RB23** and their structures.

2. 2. Biological activity

The *Mtb* InhA inhibitory effect and *Mtb* growth blocking of the synthesized compounds were tested consulting the protocols in references[22,37]. We took three controls. One was a typical InhA inhibitor Triclosan; another was a rhodanine-derived drug Epalrestat; the other was a first-line tuberculosis drug Isoniazid. In this work, two major concerns were enhancing the InhA inhibitory activity and improve the performance on *Mtb*. Seen in Table 1, in the first round, most of the compounds indicated potential for both of the demands.

Table 1. The *Mtb* InhA inhibitory and *Mtb* growth blocking activities of **RB1-RB15**.

Code	R^1	IC_{50} (μM) *Mtb* InhA	MIC (μM) *Mtb*	Code	R^1	IC_{50} (μM) *Mtb* InhA	MIC (μM) *Mtb*
RB1	-H	40.2 ± 3.25	32.3 ± 2.89	**RB9**	4-$N(Me)_2$	17.4 ± 1.42	12.6 ± 1.08
RB2	4-F	55.0 ± 5.01	57.4 ± 5.32	**RB10**	4-NHAc	11.6 ± 1.01	3.18 ± 0.29
RB3	4-Cl	50.1 ± 4.06	48.2 ± 4.61	**RB11**	2-Cl	25.8 ± 2.23	25.5 ± 2.24
RB4	4-Br	23.9 ± 1.98	21.1 ± 1.98	**RB12**	3-Cl	47.3 ± 4.28	40.9 ± 3.87
RB5	4-Me	17.5 ± 1.32	15.1 ± 1.26	**RB13**	2-OMe	28.1 ± 2.54	30.4 ± 2.53
RB6	4-OMe	8.24 ± 0.69	2.95 ± 0.27	**RB14**	3-OMe	22.6 ± 2.03	20.5 ± 1.89

RB7	4-NO_2	43.5 ± 3.78	36.5 ± 3.31	**RB15**	3,4,5-OMe	3.12 ± 0.28	0.38 ± 0.035
RB8	4-OH	35.3 ± 3.02	33.1 ± 3.05				
Triclosan		6.14 ± 0.55	8.65 ± 0.79	Epalrestat		> 200	> 200
Isoniazid		8.29 ± 0.76	0.58 ± 0.050				

Preliminary SAR studies on *Mtb* InhA was conducted according to the data in Table 1. Though the scale was not quite large, several clues could still be found. The initial one was that electron-donating groups were basically preferred at the *para*-position. The corresponding order was -OMe (**RB6**, IC_{50} = 8.24 μM) > -NHAc (**RB10**, IC_{50} = 11.6 μM) > -$N(Me)_2$ (**RB9**, IC_{50} = 17.4 μM) ≥ -Me (**RB5**, IC_{50} = 17.5 μM) > -Br (**RB4**, IC_{50} = 23.9 μM) > -OH (**RB8**, IC_{50} = 35.3 μM) > -H (**RB1**, IC_{50} = 40.2 μM) ≥ -NO_2 (**RB7**, IC_{50} = 43.5 μM) > -Cl (**RB3**, IC_{50} = 50.1 μM) > -F (**RB2**, IC_{50} = 55.0 μM). The second one came when we fixed the substitute but changed its position. For the electron-donating group (here was -OMe), the tendency was *para*- (**RB6**, IC_{50} = 8.24 μM) > *meta*- (**RB14**, IC_{50} = 22.6 μM) > *ortho*- (**RB13**, IC_{50} = 28.1 μM); whereas for the electron-withdrawing one (here was -Cl), the tendency was a opposite *ortho*- (**RB11**, IC_{50} = 25.8 μM) > *meta*- (**RB12**, IC_{50} = 47.3 μM) ≥ *para*- (**RB3**, IC_{50} = 50.1 μM). The last clue was for multi-substituted situation. Since electron-donating seemed better for this series, we picked the 3,4,5-trimethoxyl one. It suggested better potency (**RB15**, IC_{50} = 3.12 μM) than single-substituted ones.

Table 2. The *Mtb* InhA inhibitory and *Mtb* growth blocking activities of **RB16-RB23**.

Code	R^1	IC_{50} (μM) *Mtb* InhA	MIC (μM) *Mtb*	Code	R^1	IC_{50} (μM) *Mtb* InhA	MIC (μM) *Mtb*
RB16	4-F	20.1 ± 1.97	17.8 ± 1.52	**RB20**	2-Cl	15.3 ± 1.22	7.83 ± 0.72
RB17	4-Cl	16.5 ± 1.32	8.62 ± 0.76	**RB21**	3-Cl	7.84 ± 0.65	2.02 ± 0.19
RB18	4-Br	12.1 ± 1.08	4.04 ± 0.36	**RB22**	2-OMe	16.8 ± 1.41	9.27 ± 0.87
RB19	4-Me	5.02 ± 0.39	0.49 ± 0.042	**RB23**	3,4,5-OMe	2.55 ± 0.20	0.29 ± 0.025
Triclosan		6.14 ± 0.55	8.65 ± 0.79	Epalrestat		> 200	> 200
Isoniazid		8.29 ± 0.76	0.58 ± 0.050				

A second round was linked up by introducing the preferred electron-donating group from Group A to Group B and giving a brief discussion on the reset Group A (Table 2). This optimization was consulting both the above mentioned biological activities and the later elaborated molecular docking results. An obvious progress in potency could be indicated when the substitutes of Group A were the same. The requirement for electron-donating substitute still existed with the observed tendency of -Me (**RB19**, IC_{50} = 5.02 μM) > -Br (**RB18**, IC_{50} = 12.1 μM) > -Cl (**RB17**, IC_{50} = 16.5 μM) > -F (**RB16**, IC_{50} = 20.1 μM). The preference for substituent position seemed interfered because the *ortho*- or *meta*-substituted compounds (**RB20**, **RB21**, **RB22**) all suggested considerable potency. The top choice was still the 3,4,5-trimethoxyl one with potential InhA inhibitory activity (**RB23**, IC_{50} = 2.55 μM). Moreover, it was cheerful that the growth-blocking effect on *Mtb* was improved. It was still a slight pity that the top hits were subjected to antibacterial activity, which is a common phenomenon mainly due to the complex compensatory mechanism of bacteria to resist the drug action.

Top five compounds (**RB23**, **RB15**, **RB19**, **RB21** and **RB6**) were chosen for the evaluation of broad-spectrum antibacterial potency and cytotoxicity. The Gram-positive MSSA (methicillin-sensitive *Staphylococcus aureus* ATCC 25923), MRSA (methicillin-resistant *Staphylococcus aureus* ATCC 29213) and Gram-negative (*Pseudomonas aeruginosa* ATCC 27583) pathogenic bacteria were employed for the former while 293T (human embryonic kidney cell line) was recruited for the latter. As presented in Table 3, the representatives indicated potent broad-spectrum antibacterial ability and low toxicity.

Table 3. Broad-spectrum antibacterial and cytotoxic evaluation of top hits.

Compounds	MIC (μM) MSSA	MIC (μM) MRSA	MIC (μM) *P. aeruginosa*	IC_{50} (μM) 293T
RB23	1.24 ± 0.10	1.54 ± 0.13	0.95 ± 0.09	> 200

RB15	4.61 ± 0.45	7.20 ± 0.69	5.41 ± 0.44	> 200
RB19	6.15 ± 0.51	10.2 ± 0.85	8.12 ± 0.75	195 ± 18.5
RB21	2.16 ± 0.18	3.88 ± 0.28	5.05 ± 0.35	> 200
RB6	4.28 ± 0.36	4.15 ± 0.40	4.83 ± 0.43	167 ± 15.0
Triclosan	0.39 ± 0.03	0.68 ± 0.06	1.25 ± 0.11	20.5 ± 2.00
Isoniazid	1.26 ± 0.11	1.42 ± 0.12	2.85 ± 0.23	120 ± 10.5

For further determine the molecular target, two more reported antibacterial targets were included. One was DNA gyrase[40], the most common target for antibiotics, while the other was FabH[41], the fatty acid biosynthesis related enzyme. Seen in Table 4, the representatives did not indicated obvious inhibition against these two targets, thus inferred the selectivity for InhA to some degree.

Table 3. The inhibitory capability against DNA gyrase and FabH of top hits.

Code	IC_{50} (μM) DNA gyrase	IC_{50} (μM) FabH	Code	IC_{50} (μM) DNA gyrase	IC_{50} (μM) FabH
RB23	> 1000	900 ± 80	**RB15**	> 1000	780 ± 70
Triclosan	> 1000	850 ± 70	Isoniazid	> 1000	> 1000

2. 3. *In silico* study

The preliminary evaluation for the basic druggability was performed by examining the ADMET (Absorption, Distribution, Metabolism, Excretion, Toxicity) properties (Figure 2A). The AlogP (the partition coefficient of drug in octanol/aqueous solution calculated by ACD/PhysChem Suite Software) and PSA_2D (the fast calculated polar surface area from the 2D structure) were used to predict the Absorption (human intestinal absorption) and BBB (blood-brain barrier penetration) including 95% and 99% confidence ellipses as referenced.[42] All the compounds showed attractive pharmacokinetics potential which could lead to further applications.

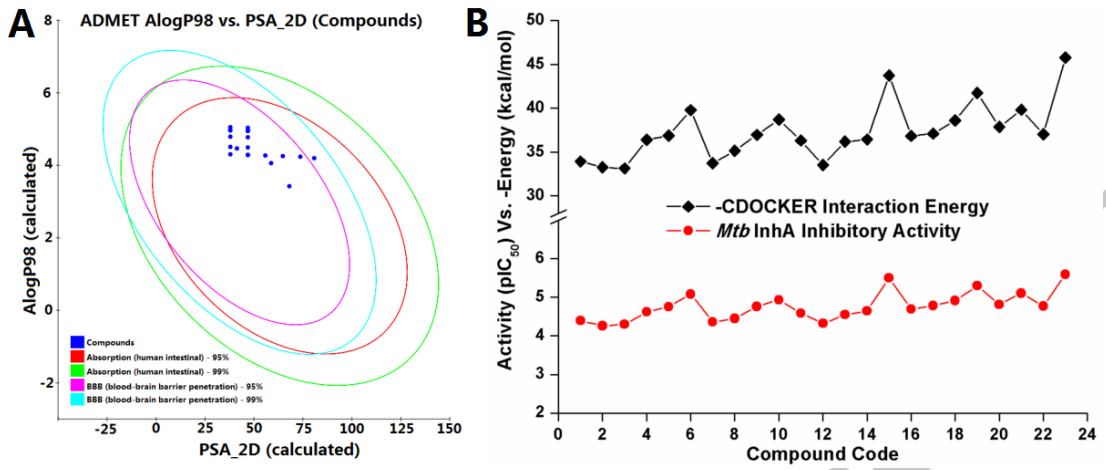

Figure 2. (A) The ADMET properties predicted for **RB1-RB23** indicated potential druggability by locating inside the innermost oval (except **RB7**); (B) The consistency between the *Mtb* InhA inhibitory activity and the negative values of calculated interaction energy.

Molecular docking simulation was performed to reveal the probable binding patterns of the synthesized compounds. The active site of *Mtb* InhA (PDB code: 4R9S) was defined as the binding site. The *Mtb* InhA inhibitory activity and the negative values of calculated interaction energy presented basically consistency (Figure 2B). This parameter together with the binding patterns and bioactivities, helped us to optimize from the first round to the second. For the first round, the 2D maps of **RB6**, **RB15** and Isoniazid within the binding position were displayed in Figure 3. We used a more recent reported crystal structure of InhA than that in the related work (PDB code: 1P45)[37]. Compared with the previous work, the residues to form the key interactions were similar but not exactly the same. They include Ser20, Phe149, Lys165 and Thr196. Meanwhile, the positions of the key interactions were not exactly fixed. This might infer the rotation of the two groups around rhodanine. In detail, **RB6** interacted with InhA via a potential hydrogen bond with Lys165 from the linker of Group B (O···H-N: 1.81 Å, 130.884°) and π-π interactions with Phe149 from rhodanine (distance: 5.14 Å). However, for **RB15**, the hydrogen bond with Lys165 moved to the *meta*-methoxyl on Group A (O···H-N: 1.89 Å, 153.584°) and the linker of Group B inferred another potential hydrogen bond with Thr196 (O···H-O: 1.95 Å, 160.955°).

Before confirming possible adduct with NAD^+, Isoniazid also presented a similar hydrogen bond with Lys165 (O···H-N: 2.03 Å, 122.105°) and another potential one with ASP148 (N-H···O: 2.05 Å, 138.026°). The binding position, as reported, was close to Tyr158 and NAD^+. For the second round, the top hit **RB23** indicated the probable hydrogen bonds with Lys165 from the linker of Group B (O···H-N: 1.73 Å, 167.410°) and with Thr196 from the *meta*-methoxyl on Group A (O···H-O: 2.14 Å, 154.123°). It also retained the π-π interactions with Phe149 from rhodanine (distance: 5.63 Å) and the close steric distance to the reported residue Ser20.

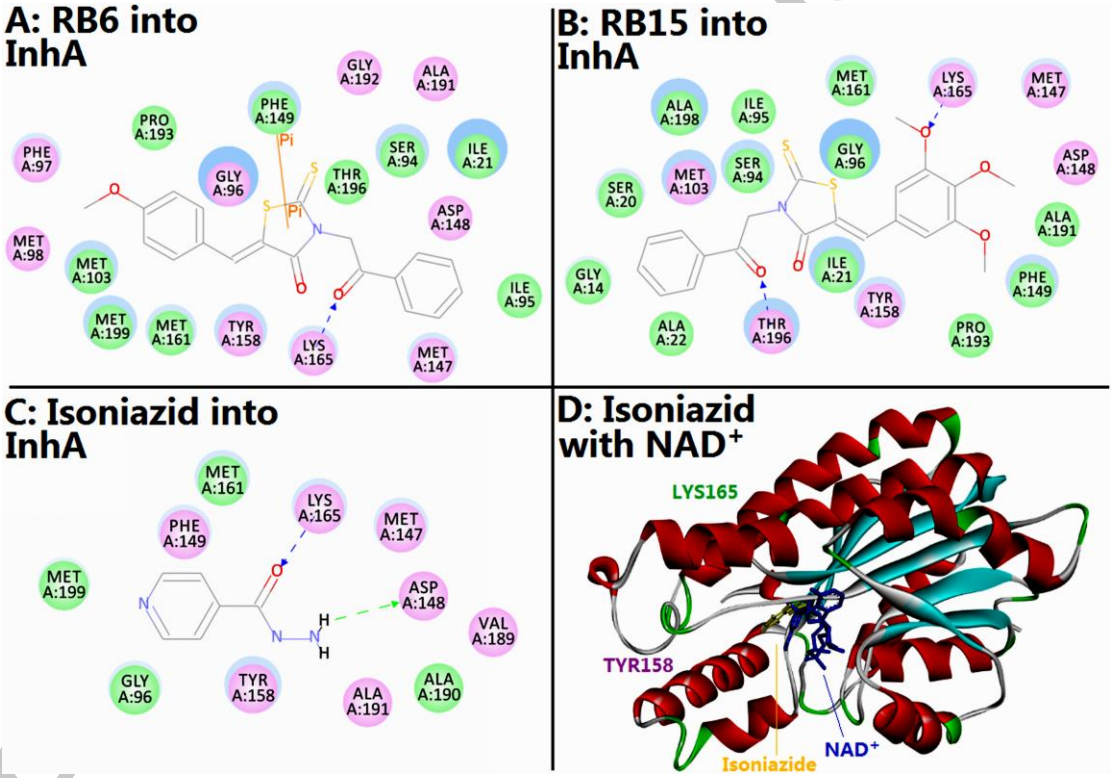

Figure 3. The 2D docking patterns of the first round representatives (A) **RB6**, (B) **RB15** and (C) Isoniazid into *Mtb* InhA. Significant interactions and residues were exhibited. The H-bonds were displayed as dotted lines. The π-π interactions were shown as orange line. (D) 3D pattern of Isoniazid with NAD^+ within InhA.

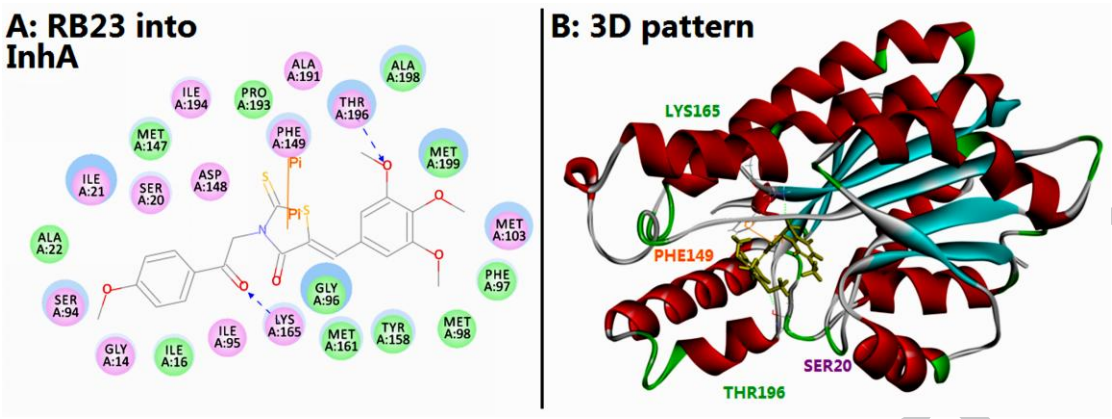

Figure 4. (A) The 2D and (B) 3D docking patterns the second round representative **RB23** into *Mtb* InhA. Significant interactions and residues were exhibited. The H-bonds were displayed as dotted lines. The π-π interactions were shown as orange line.

Moreover, the receptor surface model was generated in Figure 5A to visualize the surrounding electronic conditions of the binding pocket. Then the two referenced compounds in Figure 1 were put together with our series to participate a molecular overlay. The result in Figure 5B suggested a reliable consistency to guarantee the feasibility of the following QSAR model.

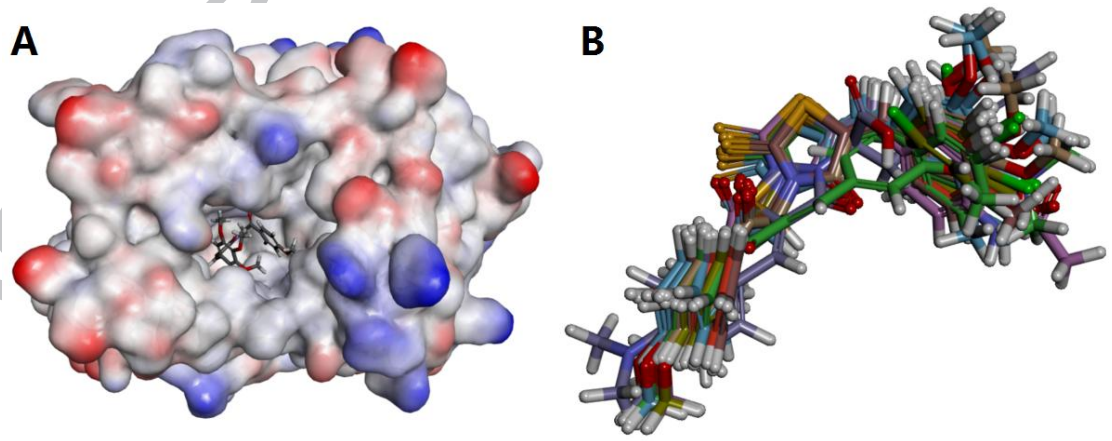

Figure 5. (A) The receptor surface model of **RB23** into *Mtb* InhA; (B) The molecular overlay of reference and our compounds indicated reliable consistency.

The 3D QSAR model was built according to the docked structures and the pIC_{50} scale (-log IC_{50}) of their InhA inhibitory activities. The correlation coefficient r^2

(0.996) ensured that the model was reliable. The electrostatic and *Van der Waals* maps were presented in Figure 6. According to the electron-withdrawing (red), electron-donating (blue), steric bulky (green) or small (yellow) requirements, the modification of this series could be induced as the following points. Since the rotation around the rhodanine moiety might exist, here Group A and B suggested the similar requirements. Seen in a more brief view Figure 6C, they both preferred an electron-donating and smaller substitute to stretch further but electron-withdrawing and larger ones to fill in the near surrounding. This result basically agreed with the above mentioned SAR discussion. Thus, a series of modification near the rhodanine moiety might be a promising orientation to perform deeper design.

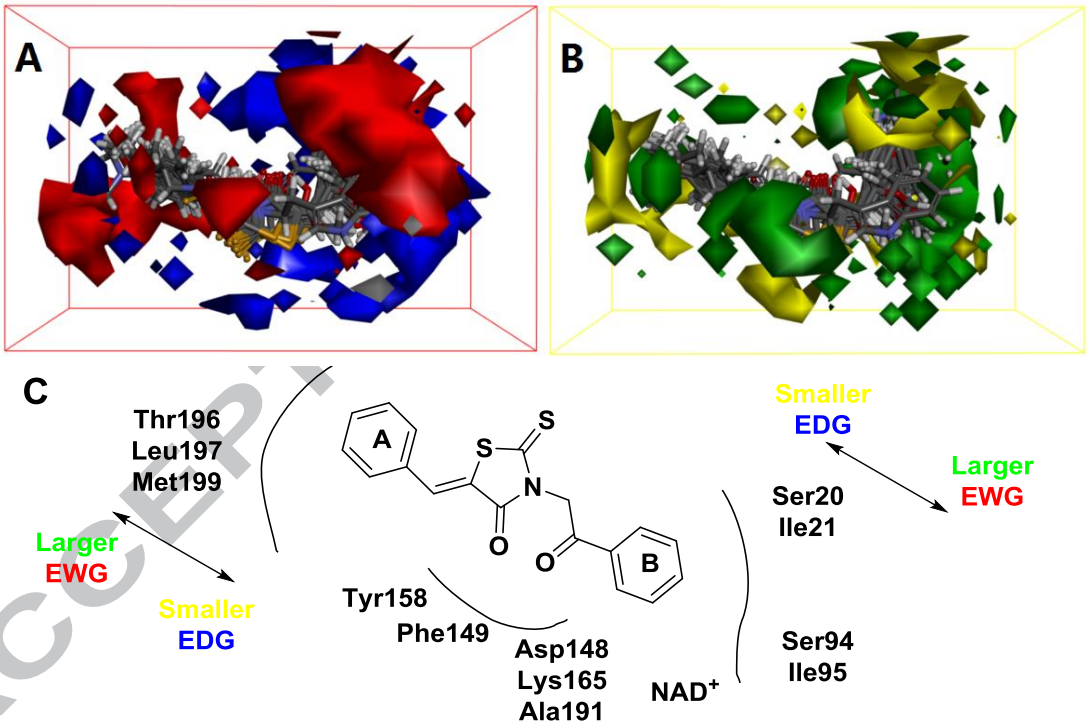

Figure 6. 3D-QSAR models of our series together with the referenced compounds (A & B) and a brief view of the modification requirements (C). The maps of electronic potential (A) and *Van der Waals* grids (B) visualized the requirements of each factor.

3. Conclusions

In summary, a two-round screening on rhodanine based series **RB1**-**RB23** was conducted to seek potential InhA inhibitory hit compounds. They were all novel

structures with their *Mtb* InhA inhibitory effect and *Mtb* growth blocking evaluated for the first time. Among them, the most potent candidate **RB23** provided comparable activities against InhA and *Mtb* with the positive control Triclosan and Isoniazid. It was also low toxic upon human embryonic cells. The ADMET analysis indicated the practical druggability of the synthesized series. The docking simulation revealed the possible binding patterns with the key residues picked as Ser20, Phe149, Lys165 and Thr196. Then the 3D-QSAR model visualized the connection between activity data and binding conformations. It would be a promising attempt to modify the surroundings near rhodanine moiety to raise future designs.

4. Experimental Section

4. 1. Chemistry

4. 1. 1. General

All the commercially available chemicals were used directly as received without further purification. All the melting points were determined on a WRS-1C digital melting point apparatus and were uncorrected. ^{1}H NMR and ^{13}C NMR spectra were recorded on a Bruker AM 600 (Rhenistetten-Forchheim, Germany) spectrometer. Shifts are reported in parts per million based on residual solvent peaks (for ^{1}H or ^{13}C/$CDCl_3$). NMR data were resolved with MestreNova software. Mass spectra were obtained from an Agilent 6540 UHD Accurate Mass Q-TOF LC/MS.

4. 1. 2. Compounds

General method of synthesis of Intermediates B

Various substituted benzaldehydes (1 mmol) were added to the rhodanine (1 mmol) alcohol solution (10 mL), respectively. Then urea (1.5 mmol) was added and the reaction continued in reflux for 5 h. After confirming the completion of the reaction by thin layer chromatography, the sediment was filtered, washed with ethanol and dried to obtain intermediates **B**.

The synthesis of (*E*)-5-arylidene-3-(2-aryl-2-oxoethyl)-2-thioxothiazolidin-4-one (RB1-RB23)

Initially, the intermediates **B** (1 mmol) were dissolved in heated ethanol (8 mL), respectively. The ethanol solution (2 mL) of different bromoacetophenones (1 mmol) and sodium ethylate (1.5 mmol) was added dropwise. The mixture was kept reacting overnight at 55 ℃. Finally the target compounds **RB1-RB23** were achieved via column chromatography and refined by recrystallization. Detailed NMR spectra were organized in "Supporting Information".

(*E*)-5-benzylidene-3-(2-oxo-2-phenylethyl)-2-thioxothiazolidin-4-one (RB1)

Yellow solid; m.p. 135-137 ℃; yield: 87%; ^{1}H NMR (600 MHz, DMSO-d_6) δ 8.09-8.08 (m, 2H), 7.88 (s, 1H), 7.74 (t, *J* = 7.4 Hz, 1H), 7.68 (d, *J* = 7.3 Hz, 2H), 7.61 (t, *J* = 7.9 Hz, 2H), 7.57 (t, *J* = 7.0 Hz, 2H), 7.54-7.51 (m, 1H), 5.29 (s, 2H); ^{13}C NMR (151 MHz, DMSO) δ 192.08, 192.04, 136.03, 135.46, 134.58, 133.60, 131.52, 130.96, 129.92, 129.43, 129.02, 126.55, 42.28; HRMS (ESI-TOF) m/z: $[M+H]^+$ Calcd. for $C_{18}H_{14}NO_2S_2$ 340.4450, Found 340.4454.

(*E*)-5-(4-fluorobenzylidene)-3-(2-oxo-2-phenylethyl)-2-thioxothiazolidin-4-one (RB2)

Yellow solid; m.p. 112-114 ℃; yield: 81%; ^{1}H NMR (600 MHz, DMSO-d_6) δ 8.10-8.08 (m, 2H), 7.90 (s, 1H), 7.77-7.72 (m, 3H), 7.61 (t, *J* = 5.8 Hz, 2H), 7.44-7.40 (m, 2H), 5.29 (s, 2H); ^{13}C NMR (151 MHz, DMSO) δ 192.06, 191.91, 179.19, 164.57, 162.90, 135.45, 134.95, 134.59, 133.51, 133.45, 130.33, 130.31, 129.44, 129.01, 126.32, 126.31, 117.21, 117.06, 58.14, 42.28; HRMS (ESI-TOF) m/z: $[M+H]^+$ Calcd. for $C_{18}H_{13}FNO_2S_2$ 358.4354, Found 357.4356.

(*E*)-5-(4-chlorobenzylidene)-3-(2-oxo-2-phenylethyl)-2-thioxothiazolidin-4-one (RB3)

Yellow solid; m.p. 171-172 ℃; yield: 88%; ^{1}H NMR (600 MHz, $CDCl_3$) δ 8.07-8.06 (m, 2H), 7.85 (s, 1H), 7.69-7.67 (m, 1H), 7.55 (t, *J* = 7.9 Hz, 2H), 7.50-7.47 (m, 4H), 5.15 (s, 2H); ^{13}C NMR (151 MHz, DMSO) δ 192.04, 191.99, 179.15, 136.11, 135.44, 134.64, 134.60, 132.56, 130.00, 129.44, 129.01, 127.26, 42.34; HRMS (ESI-TOF) m/z: $[M+H]^+$ Calcd. for $C_{18}H_{13}ClNO_2S_2$ 374.8980, Found 373.8975.

(*E*)-5-(4-bromobenzylidene)-3-(2-oxo-2-phenylethyl)-2-thioxothiazolidin-4-one (RB4)

Yellow solid; m.p. 139-141 ℃; yield: 82%; ^{1}H NMR (600 MHz, DMSO-d_6) δ 8.09-8.08 (m, 2H), 7.85 (s, 1H), 7.78-7.76 (m, 2H), 7.75-7.73 (m, 1H), 7.63-7.60 (m, 4H), 5.29 (s, 2H); ^{13}C NMR (151 MHz, DMSO) δ 192.04, 191.94, 179.16, 135.45, 134.75, 134.60, 132.93, 132.86, 132.69, 129.44, 129.02, 127.32, 125.10, 42.35.; HRMS (ESI-TOF) m/z: $[M+H]^+$ Calcd. for $C_{18}H_{13}BrNO_2S_2$ 419.3405, Found 419.3401.

(*E*)-5-(4-methylbenzylidene)-3-(2-oxo-2-phenylethyl)-2-thioxothiazolidin-4-one (RB5)

Yellow solid; m.p. 125-127 ℃; yield: 85%; ^{1}H NMR (600 MHz, DMSO-d_6) δ 8.10-8.08 (m, 2H), 7.84 (s, 1H), 7.74 (t, *J* = 7.4 Hz, 1H), 7.61 (t, *J* = 8.0 Hz, 2H), 7.57 (d, *J* = 8.1 Hz, 2H), 7.38 (d, *J* = 9.0 Hz, 2H), 5.28 (s, 2H), 2.38 (s, 3H); ^{13}C NMR (151 MHz, DMSO) δ 192.11, 191.65, 179.32, 142.03, 136.17, 135.48, 134.58, 131.06, 130.86, 130.58, 129.43, 129.01, 125.36, 42.20, 21.62; HRMS (ESI-TOF) m/z: $[M+H]^+$ Calcd. for $C_{19}H_{16}NO_2S_2$ 354.4720, Found 354.4723.

(*E*)-5-(4-methoxybenzylidene)-3-(2-oxo-2-phenylethyl)-2-thioxothiazolidin-4-one (RB6)

Brown solid; m.p. 63-65 ℃; yield: 79%; ^{1}H NMR (600 MHz, DMSO-d_6) δ 8.10-8.08 (m, 2H), 7.83 (s, 1H), 7.74 (t, *J* = 7.4 Hz, 1H), 7.66-7.64 (m, 2H) ,7.61 (t, *J* = 7.9 Hz, 2H), 7.14-7.12 (m, 2H), 5.28 (s, 2H), 3.85 (s, 3H); ^{13}C NMR (151 MHz, $CDCl_3$) δ 191.63, 190.47, 180.10, 161.88, 136.65, 134.84, 134.36, 132.68, 129.00, 128.64, 126.12, 123.42, 114.91, 55.56, 42.53; HRMS (ESI-TOF) m/z: $[M+H]^+$ Calcd. for $C_{19}H_{16}NO_3S_2$ 370.4713, Found 370.4710.

(*E*)-5-(4-nitrobenzylidene)-3-(2-oxo-2-phenylethyl)-2-thioxothiazolidin-4-one (RB7)

Brown solid; m.p. 66-68 ℃; yield: 72%; ^{1}H NMR (600 MHz, $CDCl_3$) δ 8.27-8.25 (m, 2H), 7.98-7.97 (m, 2H), 7.82 (s, 1H), 7.62-7.58 (m, 3H), 7.47 (t, *J* = 8.0 Hz, 2H), 5.08 (s, 2H); ^{13}C NMR (151 MHz, DMSO) δ 195.07, 192.53, 191.95, 178.89, 148.26, 139.90, 134.62, 133.16, 131.80, 129.44, 129.25, 129.02, 124.82, 42.56; HRMS (ESI-TOF) m/z: $[M+H]^+$ Calcd. for $C_{18}H_{13}N_2O_4S_2$ 385.4423 Found 385.4425.

(*E*)-5-(4-hydroxybenzylidene)-3-(2-oxo-2-phenylethyl)-2-thioxothiazolidin-4-one (RB8)

Yellow solid; m.p. 133-135 ℃; yield: 83%; ^{1}H NMR (600 MHz, DMSO-d_6) δ 10.46 (s, 1H), 8.10-8.08 (m, 2H), 7.78 (s, 1H), 7.74 (t, *J* = 7.4 Hz, 1H), 7.61 (t, *J* = 7.7 Hz, 2H), 7.54 (d, *J* = 8.7 Hz, 2H), 6.94 (d, *J* = 8.6 Hz, 2H), 5.27 (s, 2H); ^{13}C NMR (151 MHz, DMSO) δ 192.18, 190.66, 179.52, 161.10, 136.72, 135.51, 134.55, 133.56, 129.42, 129.00, 124.50, 122.21, 116.99, 42.06; HRMS (ESI-TOF) m/z: $[M+H]^+$ Calcd. for $C_{18}H_{14}NO_3S_2$ 356.4443, Found 356.4446.

(*E*)-5-(4-(dimethylamino)benzylidene)-3-(2-oxo-2-phenylethyl)-2-thioxothiazolidin-4-one (RB9)

Yellow solid; m.p. 126-128 ℃; yield: 87%; ^{1}H NMR (600 MHz, DMSO-d_6) δ 8.10-8.08 (m, 2H), 7.75-7.72 (m, 2H), 7.62-7.60 (m, 2H), 7.50 (d, *J* = 9.0 Hz, 2H), 6.85-6.83 (m, 2H), 5.25 (s, 2H), 3.05 (s, 6H); ^{13}C NMR (151 MHz, DMSO) δ 192.27, 188.89, 179.63, 152.46, 137.42, 135.55, 134.53, 133.39, 129.42, 129.00, 120.30, 118.88, 112.65, 41.88; HRMS (ESI-TOF) m/z: $[M+H]^+$ Calcd. for $C_{20}H_{19}N_2O_2S_2$ 383.5136, Found 383.5141.

(*E*)-N-(4-((4-oxo-3-(2-oxo-2-phenylethyl)-2-thioxothiazolidin-5-ylidene)methyl)phenyl)acetamide (RB10)

Brown solid; m.p. 75-77 ℃; yield: 86%; ^{1}H NMR (600 MHz, DMSO-d_6) δ 10.32 (s, 1H), 8.10-8.08 (m, 2H), 7.78 (t, *J* = 6.4 Hz, 1H), 7.74 (t, *J* = 7.4 Hz, 1H), 7.63-7.60 (m, 2H), 5.28 (s, 2H), 2.10 (s, 3H); ^{13}C NMR (151 MHz, DMSO) δ 192.14, 191.21, 179.43, 169.42, 142.40, 135.93, 135.49, 134.57, 132.27, 129.43, 129.01, 127.91, 124.16, 119.64, 42.18, 24.65; HRMS (ESI-TOF) m/z: $[M+H]^+$ Calcd. for $C_{20}H_{16}N_2O_3S_2$ 396.4890, Found 396.4885.

(*E*)-5-(2-chlorobenzylidene)-3-(2-oxo-2-phenylethyl)-2-thioxothiazolidin-4-one (RB11)

White solid; m.p. 116-118 ℃; yield: 85%; ^{1}H NMR (600 MHz, DMSO-d_6) δ 8.09-8.08 (m, 2H), 7.98 (s, 1H), 7.75-7.72 (m, 1H), 7.67-7.63 (m, 2H), 7.60 (t, *J* = 8.0

Hz, 2H), 7.56-7.52 (m, 2H), 5.30 (s, 2H); ^{13}C NMR (151 MHz, DMSO) δ 192.77, 191.99, 178.71, 135.42, 135.36, 134.60, 132.83, 131.77, 130.90, 130.63, 130.21, 129.84, 129.43, 129.01, 128.74, 42.48; HRMS (ESI-TOF) m/z: $[M+H]^+$ Calcd. for $C_{18}H_{13}ClNO_2S_2$ 374.8980, Found 374.8984.

(*E*)-5-(3-chlorobenzylidene)-3-(2-oxo-2-phenylethyl)-2-thioxothiazolidin-4-one (RB12)

Yellow solid; m.p. 113-115 ℃; yield: 80%; ^{1}H NMR (600 MHz, DMSO-d_6) δ 8.09-8.08 (m, 2H), 7.86 (s, 1H), 7.75-7.72 (m, 2H), 7.62-7.57 (m, 5H), 5.29 (s, 2H); ^{13}C NMR (151 MHz, DMSO) δ 192.18, 192.02, 178.99, 135.84, 135.44, 134.58, 134.52, 134.26, 131.69, 131.00, 130.67, 129.42, 129.00, 128.76, 128.26, 42.37; HRMS (ESI-TOF) m/z: $[M+H]^+$ Calcd. for $C_{18}H_{13}ClNO_2S_2$ 374.8980, Found 374.8985.

(*E*)-5-(2-methoxybenzylidene)-3-(2-oxo-2-phenylethyl)-2-thioxothiazolidin-4-one (RB13)

Yellow solid; m.p. 150-152 ℃; yield: 80%; ^{1}H NMR (600 MHz, DMSO-d_6) δ 8.09-8.08 (m, 2H), 8.03 (s, 1H), 7.75-7.72 (m, 1H), 7.61 (t, J = 8.0 Hz, 2H), 7.54-7.51 (m, 1H), 7.49-7.48 (m, 1H), 7.17 (d, J = 8.3 Hz, 1H), 7.12 (t, J = 7.5 Hz, 1H), 5.27 (s, 2H), 3.90 (s, 3H); ^{13}C NMR (151 MHz, DMSO) δ 192.12, 191.99, 179.26, 158.87, 135.48, 134.57, 133.67, 130.65, 129.86, 129.42, 129.00, 126.52, 122.03, 121.64, 112.50, 56.29, 42.12; HRMS (ESI-TOF) m/z: $[M+H]^+$ Calcd. for $C_{19}H_{16}NO_3S_2$ 370.4713, Found 370.4714.

(*E*)-5-(3-methoxybenzylidene)-3-(2-oxo-2-phenylethyl)-2-thioxothiazolidin-4-one (RB14)

Yellow solid; m.p. 182-184 ℃; yield: 92%; ^{1}H NMR (600 MHz, DMSO-d_6) δ 8.10-8.08 (m, 2H), 7.84 (s, 1H), 7.75-7.72 (m, 1H), 7.62-7.60 (m, 2H), 7.48 (t, J = 8.0 Hz, 1H), 7.25-7.23 (m, 2H), 7.11-7.09 (m, 1H), 5.29 (s, 2H), 3.81 (s, 3H); ^{13}C NMR (151 MHz, DMSO) δ 192.09, 192.07, 179.16, 160.19, 135.98, 135.47, 135.00, 134.58,

131.02, 129.43, 129.01, 126.90, 122.87, 117.43, 116.12, 55.79, 42.23; HRMS (ESI-TOF) m/z: $[M+H]^+$ Calcd. for $C_{19}H_{15}NO_3S_2$ 370.4713, Found 370.4710.

(*E*)-3-(2-oxo-2-phenylethyl)-2-thioxo-5-(3,4,5-trimethoxybenzylidene)thiazolidin-4-one (RB15)

Yellow solid; m.p. 136-138 ℃; yield: 90%; ^{1}H NMR (600 MHz, DMSO-d_6) δ 8.10-8.08 (m, 2H), 7.81 (s, 1H), 7.74 (t, *J* = 7.4Hz, 1H), 7.61 (t, *J* = 7.9 Hz, 2H), 6.98 (d, *J* = 1.4 Hz, 2H), 5.27 (s, 2H), 3.83 (s, 6H), 3.74 (s, 3H); ^{13}C NMR (151 MHz, DMSO) δ 192.09, 191.57, 179.18, 153.73, 140.43, 136.37, 135.52, 134.57, 129.43, 129.11, 128.98, 125.57, 108.46, 60.68, 56.50, 42.11; HRMS (ESI-TOF) m/z: $[M+H]^+$ Calcd. for $C_{21}H_{20}NO_5S_2$ 430.5239, Found 430.5243.

(*E)*-5-(4-fluorobenzylidene)-3-(2-(4-methoxyphenyl)-2-oxoethyl)-2-thioxothiazolidin-4-one (RB16)

Yellow solid; m.p. 168-170 ℃; yield: 80%; ^{1}H NMR (600 MHz, DMSO-d_6) δ 8.07 (t, *J* = 2.8 Hz, 1H), 8.06 (t, *J* = 1.9 Hz, 1H), 7.89 (s, 1H), 7.76-7.74 (m, 2H), 7.43-7.40 (m, 2H), 7.13-7.10 (m, 2H), 5.24 (s, 2H), 3.88 (s, 3H); ^{13}C NMR (151 MHz, $CDCl_3$) δ 191.39, 189.90, 179.84, 164.75, 164.54, 163.06, 135.09, 132.65, 132.59, 131.07, 129.85, 129.83, 127.77, 126.06, 126.04, 116.74, 116.59, 114.20, 55.66, 42.61; HRMS (ESI-TOF) m/z: $[M+H]^+$ Calcd. for $C_{19}H_{15}FNO_3S_2$ 388.4617, Found 388.4618.

(*E*)-5-(4-chlorobenzylidene)-3-(2-(4-methoxyphenyl)-2-oxoethyl)-2-thioxothiazolidin-4-one (RB17)

Yellow solid; m.p. 111-113 ℃; yield: 77%; ^{1}H NMR (600 MHz, DMSO-d_6) δ 8.07 (t, *J* = 2.9 Hz, 1H), 8.06 (t, *J* = 2.0 Hz, 1H), 7.87 (s, 1H), 7.70-7.69 (m, 2H), 7.65-7.62 (m, 2H), 7.14-7.11 (m, 2H), 5.24 (s, 2H), 3.88 (s, 3H); ^{13}C NMR (151 MHz, $CDCl_3$) δ 191.41, 189.84, 179.77, 164.55, 136.98, 134.81, 132.00, 131.60, 131.07, 129.64, 127.75, 126.90, 114.20, 55.65, 42.65; HRMS (ESI-TOF) m/z: $[M+H]^+$ Calcd. for $C_{19}H_{15}ClNO_3S_2$ 404.9243, Found 404.9239.

(*E*)-5-(4-bromobenzylidene)-3-(2-(4-methoxyphenyl)-2-oxoethyl)-2-thioxothiazolidin-4-one (RB18)

Brown solid; m.p. 65-67 ℃; yield: 75%; ^{1}H NMR (600 MHz, DMSO-d_6) δ 8.06-8.03 (m, 2H), 7.83 (s, 1H), 7.65-7.63 (m, 2H), 7.42-7.41 (m, 2H), 5.12 (s, 2H), 3.93 (s, 3H); ^{13}C NMR (151 MHz, $CDCl_3$) δ 191.43, 189.84, 179.78, 164.55, 134.87, 132.60, 132.41, 131.73, 131.07, 127.75, 127.03, 125.44, 114.20, 58.51, 55.65, 42.65, 18.46; HRMS (ESI-TOF) m/z: $[M+H]^+$ Calcd. for $C_{19}H_{15}BrNO_3S_2$ 449.3669, Found 449.3666.

(*E*)-3-(2-(4-methoxyphenyl)-2-oxoethyl)-5-(4-methylbenzylidene)-2-thioxothiazolidin-4-one (RB19)

Yellow solid; m.p. 145-147 ℃; yield: 81%; ^{1}H NMR (600 MHz, DMSO-d_6) δ 8.08-8.06 (m, 2H), 7.83 (s, 1H), 7.57 (d, *J* = 8.1 Hz, 2H), 7.38 (d, *J* = 8.0 Hz, 2H), 7.13-7.11 (m, 2H), 5.23 (s, 2H), 3.86 (s, 3H), 2.38 (s, 3H) ; ^{13}C NMR (151 MHz, DMSO) δ 191.77, 190.38, 179.39, 164.30, 142.00, 136.08, 131.46, 131.06, 130.87, 130.58, 128.32, 125.39, 114.64, 56.18, 41.99, 21.62; HRMS (ESI-TOF) m/z: $[M+H]^+$ Calcd. for $C_{20}H_{18}NO_3S_2$ 384.4983, Found 384.4979.

(*E*)-5-(2-chlorobenzylidene)-3-(2-(4-methoxyphenyl)-2-oxoethyl)-2-thioxothiazolidin-4-one (RB20)

Brown solid; m.p. 55-57 ℃; yield: 80%; ^{1}H NMR (600 MHz, DMSO-d_6) δ 8.07 (t, *J* = 1.8 Hz, 1H), 8.05 (t, *J* = 2.1 Hz, 1H), 7.99 (s, 1H), 7.67-7.64 (m, 2H), 7.55-7.53 (m, 2H), 7.12-7.10 (m, 2H), 5.24 (s, 2H), 3.88 (s, 3H); ^{13}C NMR (151 MHz, $CDCl_3$) δ 191.88, 189.88, 179.17, 164.55, 136.41, 132.30, 132.22, 131.54, 131.08, 130.51, 129.42, 129.24, 127.74, 127.37, 114.20, 55.66, 42.65; HRMS (ESI-TOF) m/z: $[M+H]^+$ Calcd. for $C_{19}H_{15}ClNO_3S_2$ 404.9243, Found 404.9238.

(*E*)-5-(3-chlorobenzylidene)-3-(2-(4-methoxyphenyl)-2-oxoethyl)-2-thioxothiazolidin-4-one (RB21)

Brown solid; m.p. 55-57 ℃; yield: 80%; ^{1}H NMR (600 MHz, $CDCl_3$) δ 8.05-8.03 (m, 2H), 7.81 (s, 1H), 7.51 (s, 1H), 7.44-7.42(m, 3H), 7.01-6.99 (m, 2H), 5.11 (s, 2H), 3.92 (s, 3H); ^{13}C NMR (151 MHz, CDCl3) δ 191.71, 189.80, 179.60, 164.54, 135.38, 135.33, 134.45, 131.06, 130.65, 130.50, 130.06, 128.41, 127.89, 127.74, 114.20,

58.50, 55.65, 42.68, 18.46; HRMS (ESI-TOF) m/z: $[M+H]^+$ Calcd. for $C_{19}H_{15}ClNO_3S_2$ 404.9243, Found 404.9240.

(*E*)-5-(2-methoxybenzylidene)-3-(2-(4-methoxyphenyl)-2-oxoethyl)-2-thioxothiazolidin-4-one (RB22)

Brown solid; m.p. 55-57 ℃; yield: 80%; ^{1}H NMR (600 MHz, DMSO-d_6) δ 8.06 (d, *J* = 7.4 Hz, 2H), 8.03 (s, 1H), 7.53-7.49 (m, 2H), 7.18 (d, *J* = 7.7 Hz, 1H), 7.11 (d, *J* = 7.5 Hz, 3H), 5.22 (s, 2H), 3.91 (s, 3H), 3.88 (s, 3H); ^{13}C NMR (151 MHz, $CDCl_3$) δ 191.42, 190.14, 179.96, 164.48, 158.91, 132.65, 132.02, 131.07, 129.77, 127.83, 126.24, 122.77, 120.98, 114.15, 111.20, 55.64, 55.55, 42.36; HRMS (ESI-TOF) m/z: $[M+H]^+$ Calcd. for $C_{20}H_{18}NO_4S_2$ 400.4976, Found 400.4975.

(*E*)-3-(2-(4-methoxyphenyl)-2-oxoethyl)-2-thioxo-5-(3,4,5-trimethoxybenzylidene) thiazolidin-4-one (RB23)

Brown solid; m.p. 55-57 ℃; yield: 80%; ^{1}H NMR (600 MHz, DMSO-d_6) δ 8.08-8.06 (m, 2H), 7.81 (s, 1H), 7.13-7.10 (m, 2H), 6.99 (s, 2H), 5.22 (s, 2H), 3.89 (s, 3H), 3.83 (s, 6H), 3.74 (s, 3H); ^{13}C NMR (151 MHz, DMSO) δ 191.72, 190.35, 179.24, 164.30, 153.74, 140.42, 136.28, 131.43, 129.14, 128.37, 125.62, 114.64, 108.45, 60.73, 56.50, 56.18, 41.87; HRMS (ESI-TOF) m/z: $[M+H]^+$ Calcd. for $C_{22}H_{22}NO_6S_2$ 460.5502, Found 460.5498.

4. 2. Biological assay

4. 2. 1. Minimum inhibitory concentration

The minimun inhibitory concentrations were determined according to the references.[22,37] *Mtb* was grown in a 7H9 medium with OADC for 24 h at 37 ℃ under microaerobi conditions (5% O_2, 10% CO_2, and 85% N_2). The other strains Methicillin-sensitive *Staphylococcus aureus* ATCC 25923, methicillin-resistant *Staphylococcus aureus* ATCC 29213 and *Pseudomonas aeruginosa* ATCC 27583 were grown in Brucella Broth supplemented with 10% heat-inactivated horse serum. Inoculums containing 1×10^5 bacteria were seeded in 96 well plates with different concentrations of test compounds and incubated at 37 ℃ for 48 h. Absorbance was

measured at 590 nm. Wells without test compounds and with media only served as control and blank, respectively. The percentages of growth inhibition were calculated, and the concentrations of compounds producing 80% inhibition were considered as MIC values.

4. 2. 2. *Mtb* InhA inhibition assay

The standard method in references was used.[22,37] After the expression, purification, ultrasonication and SDS-PAGE procedure, *Mtb* InhA was collected. Then *Mtb* InhA inhibition was measured by monitoring the initial velocities (120 s) of the decrease in the absorbance of NADH at 340 nm, 25 ℃. The standard reaction mixture of 1.0 mL included buffer (30 mM PIPES, 150 mM NaCl, 1 mM EDTA, pH 6.8), 200 μM *trans*-2-decenoyl-*N*-acetyl cysteamine, 100 μM NADH and 1 μg recombinant *Mtb* InhA. The data of positive control was close to literature value. All assays were performed in triplicates.

4. 2. 3. DNA gyrase and FabH inhibition assay

The standard protocols of DNA gyrase[40] and FabH[41] inhibition assays in references were used respectively.

4. 3. Cytotoxicity

293T (human embryonic kidney cell line) was used for cytotoxicity evaluation via MTT method according to reference.[43]

4. 4. *In silico* assay

The Chem. 3D ultra 14.0 software [Chemical Structure Drawing Standard; Cambridge Soft corporation, USA (2014)] was employed to construct the three-dimensional structures of the aforementioned compounds. The CHARMm based force field was recruited for minimization and molecular docking simulation. The ADMET study was conducted by Calculate Molecular Properties in Small Molecules module of Discovery Studio 3.5 (Accelrys, Inc. San Diego, CA). The ADMET properties map and data were provided by the ADMET Descriptors tool. Molecular docking was carried out by CDOCKER protocol as described.[43] In this work, the structures of *Mtb* InhA (PDB code: 4R9S) was used as the receptor. 3D-QSAR model was built consulting the reference.[44] After selecting the training set and the test set

(20%, **RB5**, **RB8**, **RB10**, **RB13** and **RB15**), the Create 3D QSAR Model protocol was used to provide a reliable 3D-QSAR model with visualized electrostatic and *Van der Waals* potential maps.

Acknowledgment

This work was supported by the Major Science and Technology Program for Water Pollution Control and Treatment, China (No. 2017ZX07602-002), the Public Science and Technology Research Funds Projects of Ocean (No. 201505023), and the National Natural Science Foundation of China (No. 21602103).

Conflict of Interest The authors declare no conflict of interest.

Supporting Information The NMR data of synthesized compounds.

References and notes

1. Parsonnet J, Friedman GD, Vandersteen DP, Chang Y, Vogelman JH, Orentreich N, Sibley RK. *N. Engl. J. Med.* 1991; 325: 1127-1131.
2. Holden MTG, Feil EJ, Lindsay JA, Peacock SJ, Day NPJ, Enright MC, Foster TJ, Moore CE, Hurst L, Atkin R, et al. *Proc. Nat. Acad. Sci. USA* 2004; 101: 9786-9791.
3. Gao RB, Cao B, Hu YW, Feng ZJ, Wang DY, Hu WF, Chen J, Jie ZJ, Qiu HB, Xu K, et al. *N. Engl. J. Med.* 2013; 368: 1888-1897.
4. Bi E, Lutkenhaus J. *Nature* 1991; 354: 161-164.
5. Higashi H, Tsutsumi R, Muto S, Sugiyama T, Azuma T, Asaka M, Hatakeyama M. *Science* 2002; 295: 683-686.
6. Le Poul E, Loison C, Struyf S, Springael JY, Lannoy V, Decobecq ME, Brezillon S, Dupriez V, Vassart G, Van Damme J, Parmentier M, Detheux M. *J. Biol. Chem.* 2003; 278: 25481-25489.
7. Wang J, Soisson SM, Young K, Shoop W, Kodali S, Galgoci A, Painter R, Parthasarathy G, Tang YS, Cummings R, et al. *Nature*, 2006; 441: 358-361.
8. Heath RJ, Yu YT, Shapiro MA, Olson E, Rock CO. *J. Biol. Chem.* 1998; 273:

30316-30320.

9. Vilcheze C, Morbidoni HR, Weisbrod TR, Iwamoto H, Kuo M, Sacchettini JC, Jacobs WR. *J. Bacteriol.* 2000; 182: 4059-4067.
10. Rozwarski DA, Grant GA, Barton DHR, Jacobs WR, Sacchettini JC. *Science* 1998; 279: 98-102.
11. Vilcheze C, Wang F, Arai M, Hazbon MH, Colangeli R, Kremer L, Weisbrod TR, Alland D, Sacchettini JC, Jacobs WR. *Nat. Med.* 2006; 12: 1027-1029.
12. Marrakchi H, Laneelle G, Quemard A. *Microbiology* 2000; 146: 289-296.
13. McMurry LM, McDermott PF, Levy SB. *Antimicrob. Agents Ch.* 1999; 43: 711-713.
14. Parikh SL, Xiao GP, Tonge PJ. *Biochemistry* 2000; 39: 7645-7650.
15. Lei BF, Wei CJ, Tu SC. *J. Biol. Chem.* 2000; 275: 2520-2526.
16. Heath RJ, Rubin JR, Holland DR, Zhang EL, Snow ME, Rock CO. *J. Biol. Chem.* 1999; 274: 11110-11114.
17. Vosatka R, Kratky M, Vinsova J. *Eur. J. Pharm. Sci.* 2018; 114: 318-331.
18. Rozman K, Sosic I, Fernandez R, Young RJ, Mendoza A, Gobec S, Encinas L. *Drug Discov. Today* 2017; 22: 492-502.
19. He X, Alian A, Stroud R, De Montellano PRO. *J. Med. Chem.* 2006; 49: 6308-6323.
20. Pan P, Tonge PJ. *Curr. Top. Med. Chem.* 2012; 12: 672-693.
21. Spagnuolo LA, Eltschkner S, Yu WX, Daryaee F, Davoodi S, Knudson SE, Allen EKH, Merino J, Pschibul A, Moree B, et al. *J. Am. Chem. Soc.* 2017; 139: 3417-3429.
22. Suresh A, Srinivasarao S, Agnieszka N, Ewa AK, Alvala M, Lherbet C, Sekhar KVGC. *Chem. Biol. Drug Des.* 2018; 91: 1078-1086.
23. Hartkoorn RC, Pojer F, Read JA, Gingell H, Neres J, Horlacher OP, Altmann KH, Cole ST. *Nat. Chem. Biol.* 2014; 10: 96-98.
24. Hartkoorn RC, Sala C, Neres J, Pojer F, Magnet S, Mukherjee R, Uplekar S, Boy-Rottger S, Altmann KH, Cole ST. *EMBO Mol. Med.* 2012; 4: 1032-1042.
25. Koul A, Arnoult E, Lounis N, Guillemont J, Andries K. *Nature* 2011; 469:

483-490.

26. Iseman MD. *New Engl. J. Med.* 1993; 329: 784-791.
27. Mdluli K, Slayden RA, Zhu YQ, Ramaswamy S, Pan X, Mead D, Crane DD, Musser JM, Barry CE. *Science* 1988; 280: 1607-1610.
28. Rawat R, Whitty A, Tonge PJ. *Proc. Nat. Acad. Sci. USA* 2003; 100: 13881-13886.
29. Manjunatha UH, Rao SPS, Kondreddi RR, Noble CG, Camacho LR, Tan BH, Ng SH, Ng PS, Ma NL, Lakshminarayana SB, et al. *Sci. Transl. Med.* 2015; 7: 269ra3.
30. Sink R, Sosic I, Zivec, M, Fernandez-Menendez R, Turk S, Pajk S, Alvarez-Gomez D, Lopez-Roman EM, Gonzales-Cortez C, Rullas-Triconado J, et al. *J. Med. Chem.* 2015; 58: 613-624.
31. Kanetaka H, Koseki Y, Taira J, Umei T, Komatsu H, Sakamato H, Gulten G, Sacchettini JC, Kitamura M, Aoki S. *Eur. J. Med. Chem.* 2015; 94: 378-385.
32. Zervosen A, Lu WP, Chen ZL, White RE, Demuth TP, Frere JM. *Antimicrob. Agents Ch.* 2004; 48: 961-969.
33. Mariner KR, Trowbridge R, Agarwal AK, Miller K, O'Neill AJ, Fishwick CWG, Chopra I. *Antimicrob. Agents Ch.* 2010; 54: 4506-4509.
34. Villain-Guillot P, Gualtieri M, Bastide L, Roquet F, Martinez J, Amblard M, Pugniere M, Leonetti JP. *J. Med. Chem.* 2007; 50: 4195-4204.
35. Andleeb H, Tehseen Y, Jabeen F, Khan I, Iqbal J, Hameed S. *Bioorg. Chem.* 2017; 75: 1-15.
36. Kumar G, Parasuraman P, Sharma SK, Banerjee T, Karmodiya K, Surolia N, Surolia A. *J. Med. Chem.* 2007; 50: 2665-2675.
37. Slepikas L, Chiriano G, Perozzo R, Tardy S, Kranjc A, Patthey-Vuadens O, Ouertatani-Sakouhi H, Kicka S, Harrison CF, Scrignari T, et al. *J. Med. Chem.* 2016; 59: 10917-10928.
38. Senczuk L, Senczuk M, Urbanowicz M. *Pol. J. Chem.* 1982; 56: 1549-1552.
39. Xu YJ, Su MM, Li HL, Liu QX, Xu C, Yang YS, Zhu HL. *Anal. Chim. Acta* 2018; 1043: 123-131.

40. Laurin P, Ferroud D, Klich M, Dupuis-Hamelin C, Mauvais P, Lassaigne P, Bonnefoy A, Musicki B. *Bioorg. Med. Chem. Lett.* 1999; 9: 2079-2084.

41. Lee JY, Jeong KW, Lee JU, Kang DI, Kim Y. *Bioorg. Med. Chem.* 2009; 17: 1506-1513.

42. Egan WJ, Lauri G. *Adv. Drug Del. Rev.* 2002; 54: 273-289.

43. Li HL, Su MM, Xu YJ, Xu C, Yang YS, Zhu HL. *Eur. J. Med. Chem.* 2018; 155: 725-735.

44. Yang YS, Su MM, Zhang XP, Liu QX, He ZX, Xu C, Zhu HL. *Bioorg. Med. Chem. Lett.* 2018; 28: 3182-3186.

> 23 rhodanine derivatives were synthesized through a two-round screening.

> Their anti-bacterial activity was evaluated for the first time.

> The top hit showed improved growth-blocking effect on *Mtb* and low toxicity.

> Molecular docking indicated possible binding pattern and key interacted residues.

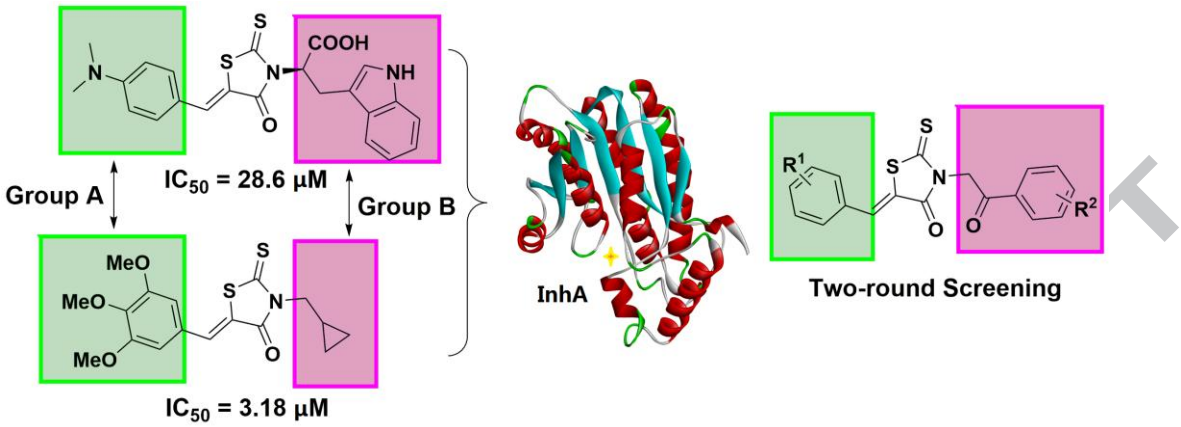

A series of rhodanine derivatives **RB1-RB23** were synthesized through a two-round screening with their *Mycobacterial tuberculosis* (*Mtb*) InhA inhibitory activity and *Mtb* growth blocking capability evaluated. The improved growth-blocking effect on *Mtb* and low toxicity were attractive for further development. The docking simulation the key interacted residues as Ser20, Phe149, Lys165 and Thr196 in the binding pattern.